


## Article

# Kinetic, Thermodynamic, and Mechanistic Studies on the Effect of the Preparation Method on the Catalytic Activity of Synthetic Zeolite-A during the Transesterification of Waste Cooking Oil

Mohamed Adel Sayed<sup>1,2</sup>, Sayed A. Ahmed<sup>1</sup>, Sarah I. Othman<sup>3</sup>, Ahmed A. Allam<sup>4</sup>, Wail Al Zoubi<sup>5</sup>, Jamaan S. Ajarem<sup>6</sup>, Mostafa R. Abukhadra<sup>2,7,\*</sup> and Stefano Bellucci<sup>8,\*</sup> 

<sup>1</sup> Department of Chemistry, Faculty of Science, Beni-Suef University, Beni-Suef 62514, Egypt

<sup>2</sup> Materials Technologies and Their Applications Laboratory, Geology Department, Faculty of Science, Beni-Suef University, Beni-Suef 62514, Egypt

<sup>3</sup> Biology Department, College of Science, Princess Nourah bint Abdulrahman University, Riyadh 11564, Saudi Arabia

<sup>4</sup> Zoology Department, Faculty of Science, Beni-Suef University, Beni-Suef 62514, Egypt

<sup>5</sup> Materials Electrochemistry Laboratory, School of Materials Science and Engineering, Yeungnam University, Gyeongsan 38541, Republic of Korea

<sup>6</sup> Zoology Department, College of Science, King Saud University, Riyadh 11362, Saudi Arabia

<sup>7</sup> Geology Department, Faculty of Science, Beni-Suef University, Beni-Suef 65211, Egypt

<sup>8</sup> INFN—Laboratori Nazionali di Frascati, 00044 Frascati, Italy

\* Correspondence: abukhadra89@science.bsu.edu.eg (M.R.A.); stefano.bellucci@lnf.infn.it (S.B.)

**Abstract:** Egyptian kaolinite was applied in the synthesis of zeolite-A by conventional hydrothermal and alkali fusion methods, resulting in two forms of zeolite-A: the hydrated phase (H.ZA) and the dehydrated phase (DH.ZA). The DH.ZA phase exhibits an enhanced surface area (488 m<sup>2</sup>/g), total basicity (7.73 mmol OH/g), high sodium content (20.2%), and a narrow particle size distribution (5 to 25 μm) as compared to the H.ZA phase (423 m<sup>2</sup>/g surface area, 5.88 mmol OH/g total basicity, 13.3% sodium content, and 10 to 45 μm particle size distribution). DH.ZA exhibits enhanced catalytic activity, achieving a biodiesel yield of 96.8% after 60 min at 60 °C, while the application of H.ZA resulted in a 95.8% yield after 120 min at 80 °C. The controlled transesterification mechanism in the presence of H.ZA and DH.ZA involved robust base-catalyzed reactions. The reactions follow the pseudo-first-order kinetics, and the rate constants ( $K_c$ ) were determined at three different temperature values (40, 50 and 60 °C). The activation energies using H.ZA (35.9 kJ·mol<sup>-1</sup>) and DH.ZA (32.714 kJ·mol<sup>-1</sup>) demonstrates their efficiencies in mild conditions. The thermodynamic parameters of enthalpy (33.23 kJ·mol<sup>-1</sup> (H.ZA) and 30.03 kJ·mol<sup>-1</sup> (DH.ZA)), Gibb's free energy (65.164 kJ·mol<sup>-1</sup> (H.ZA) and 65.268 kJ·mol<sup>-1</sup> (DH.ZA)), and entropy (−195.59 J·K<sup>-1</sup>·mol<sup>-1</sup> (H.ZA) and −195.91 J·K<sup>-1</sup>·mol<sup>-1</sup> (DH.ZA)) demonstrate the spontaneous and endothermic behaviours of these reactions. The obtained biodiesel matches the physical properties of the international standards, and the recyclability properties of the two zeolite phases demonstrate their suitability for commercial-scale applications.

**Keywords:** zeolite-A; synthesis method; transesterification; kinetics; thermodynamic; mechanism



**Citation:** Sayed, M.A.; Ahmed, S.A.; Othman, S.I.; Allam, A.A.; Al Zoubi, W.; Ajarem, J.S.; Abukhadra, M.R.; Bellucci, S. Kinetic, Thermodynamic, and Mechanistic Studies on the Effect of the Preparation Method on the Catalytic Activity of Synthetic Zeolite-A during the Transesterification of Waste Cooking Oil. *Catalysts* **2023**, *13*, 30. <https://doi.org/10.3390/catal13010030>

Academic Editors: Ning Rui and Lili Lin

Received: 4 November 2022

Revised: 17 December 2022

Accepted: 20 December 2022

Published: 24 December 2022



**Copyright:** © 2022 by the authors. Licensee MDPI, Basel, Switzerland. This article is an open access article distributed under the terms and conditions of the Creative Commons Attribution (CC BY) license (<https://creativecommons.org/licenses/by/4.0/>).

## 1. Introduction

There is rapid growth in the cost of crude oil around the world as well as its extraction processes; this is in addition to the extensive and controlled consumption of common traditional fossil fuels [1,2]. Moreover, the consumption of these fuels is associated with serious environmental concerns, which are related to the immense emissions of the essential greenhouse gases and their side impacts on the climate change phenomenon [3,4]. Therefore, the interested researchers, as well as the environmental and energy authorities, have done their best to introduce green, clean, environmental, and renewable energy supplies to

face the continuous increase in world energy demands and to match the environmental specifications of fuels [5,6]. Recently, different forms of biofuels (solid biofuels, biodiesels, and gaseous biofuels) have been assessed as sustainable, low-cost, and environmental alternatives to the commonly used traditional fossil fuels [5,6].

The commonly produced biodiesel forms exhibit biodegradable, nontoxic, sulfur-free, sustainable, low toxic emission, and commercialization properties [7–9]. The determined physical properties of biodiesel, such as its viscosity, flash point, cetane number, and calorific value, qualify most of the introduced products to be applied effectively and safely as fuel in the engines either as a single phase or as an integrated phase in a blend with the common traditional diesel [1,10,11]. Thereby, biodiesel fuels represent promising additional energy supplies and potential alternatives for the common fossil fuels to face their environmental drawbacks and match the future shortage in the traditional energy supplies in the world [12–14]. Biodiesel products are extracted widely from different types of animal fats, biomasses, algae, and agricultural feedstock, including both edible and nonedible oils of plants and vegetables [15,16]. Several recent studies demonstrated the possible extraction of biodiesel from spent or waste cooking oil, which can act as low-cost, commercial, and recyclable precursors [17].

The conversion processes of oil into the different forms of biodiesel have involved essentially transesterification reactions for the triglyceride components of oil in the presence of an effective catalyst and suitable content of alcohol-producing series of fatty acid alkyl esters (FAAEs) (biodiesel) [18]. Most of the previous studies demonstrated a controlling effect of the incorporated catalyst on the efficiencies and rates of the transesterification reactions in addition to the physical properties of the obtained biodiesel [19]. The commonly used catalysts can be divided into single-phase catalysts (homogenous catalysts) and multi-phase catalysts (heterogeneous catalysts) [20,21]. However, the commonly used one-phase catalysts, either the acidic forms (HCl and H<sub>2</sub>SO<sub>4</sub>) or the alkali forms (NaOH and KOH), exhibit considerable cost and significant activity within short conversion intervals. Their application is associated with several side effects [20,22]. The commonly reported drawbacks of the one-phase catalysts are their complex and difficult separation processes for the resulting products, their poor recyclability values, their corrosion effects, and the toxic byproducts that result during their applications [21]. On the other hand, the multi-phase or heterogeneous catalysts were assessed as recyclable materials that exhibit high recovery and non-corrosive properties in addition to their environmental value [1].

Recently, a wide range of clay-based catalysts, including ion-exchanged catalysts, acidic and basic activated clay catalysts, and clay-supported catalysts, have been developed and used [23]. The alkali (K<sup>+</sup>, Na<sup>+</sup>, Ca<sup>2+</sup>)-bearing silicate and aluminosilicate structures have been introduced as a promising group of multi-phase catalysts during the transesterification of different types of vegetable oils [3]. This is related to the availability of their precursors in addition to their low cost and simple production methods [24,25]. The synthetic zeolite forms (zeolite-P, zeolite-A, sodalite, zeolite-X, and zeolite-Y) were categorized as the most effective alkali-bearing aluminosilicate heterogeneous catalysts, either as single phases or modified phases, for their unique physicochemical properties [25–27]. Generally, synthetic zeolites are characterized by highly ordered nanoporous structures in addition to their excellent ion exchangeability, surface area, surface reactivity, thermal stability, dispersion properties, chemical and crystalline flexibility, and mechanical stability [23,27,28].

Zeolite-A (LTA type) is the most studied synthetic zeolite for different traditional and advanced applications, including water remediation, drug delivery, gas separation, filtration, detergents, and water-softening applications [23,29]. However, the catalytic activities of zeolite-A during the transesterification reactions were not covered with satisfactory studies yet as compared to the introduced studies about synthetic zeolite-X, zeolite-Y, and sodalite [28,30]. Moreover, the synthetic zeolite-A can be synthesized from different raw materials (kaolinite, rice husk, fly ash, fumed silica) by different methods and under different synthesis conditions, which significantly affect the physicochemical and catalytic

properties of the final product [26,28]. Such synthesis conditions strongly affected the morphology, chemical composition, porous structure, and crystallinity degree of the synthetic zeolite [26,31,32].

In the current study, the synthetic zeolite Na-A was produced from Egyptian kaolinite by two different methods (the conventional hydrothermal method and alkali fusion method), and its catalytic activities during the transesterification of waste cooking oil were followed in detail. The impact of the synthesis methods on the catalytic activity of the two zeolite-A forms was studied based on the experimental biodiesel production efficiency, transesterification rate, kinetic behavior, and thermodynamic studies considering the textural, morphological, and chemical properties of the two forms of zeolite.

## 2. Results and Discussion

### 2.1. Characterization of the Catalysts

#### 2.1.1. XRD Analysis

The XRD patterns of the used raw kaolinite, as well as the synthetic zeolite-A form (H.ZA and DH.ZA), are presented in Figure 1. The raw kaolinite material exhibits the typical pattern of well-crystallized kaolinite, with the identification peaks of its triclinic system at  $12.3^\circ$  (001) and  $24.9^\circ$  (002) in addition to other common peaks at  $20.8^\circ$  ( $-110$ ) and  $26.6^\circ$  (111) (Figure 1A) (XRD. No. 04-012-5104). The recognition of the thermally activated kaolinite displays the characteristic pattern of amorphous materials, confirming the transformation of kaolinite into reactive metakaolinite (Figure 1B). The XRD pattern of the synthetic zeolite by the conventional hydrothermal method reflected the significant alteration of triclinic kaolinite into cubic LTA zeolite (Zeolite-A) (Figure 1C). This was concluded based on the detected high diffraction peaks of zeolite-A at  $7.2^\circ$ ,  $10.32^\circ$ ,  $12.6^\circ$ ,  $16.2^\circ$ ,  $21.83^\circ$ ,  $24^\circ$ ,  $26.2^\circ$ ,  $27.23^\circ$ ,  $30.1^\circ$ ,  $30.9^\circ$ ,  $31.1^\circ$ ,  $32.6^\circ$ ,  $33.39^\circ$ , and  $34.3^\circ$  (Figure 1B) (Ref.Cd. No. 01-089-3142) (Figure 1C). This form was reported as a hydrated form of LTA zeolite (Zeolite-A). The obtained pattern of the sample that was prepared by the alkali fusion method also demonstrates the characteristic peaks of zeolite-A but with a dehydrated or anhydrous form (Ref.Cd. No. 01-089-5423) (Figure 1D). The remarkable peaks of both the hydrated form (H.ZA) obtained by the conventional method and the dehydrated form (DH.ZA) obtained by the alkali fusion method demonstrate the higher crystallinity of DH.ZA than H.ZA, which is in agreement with the previous studies [33,34]. Moreover, the determined crystallite size of DH.ZA (13.4 nm) is smaller than H.ZA, demonstrating the role of the fusion methods in accelerating the dissolution and nucleation rate of the aluminosilicate gel.

#### 2.1.2. FT-IR Analysis

The main functional chemical groups of the synthetic zeolite-A phases as well as their raw materials, were assessed based on their FT-IR spectra (Figure 2). The observed spectrum of kaolinite as a raw precursor reflects the main chemical groups of clay minerals, such as Si-OH ( $3689\text{ cm}^{-1}$ ), Al-OH ( $912\text{ cm}^{-1}$  and  $3622\text{ cm}^{-1}$ ), hydroxyl groups (O-H) ( $1641\text{ cm}^{-1}$ ), Si-O-Si ( $1020\text{ cm}^{-1}$ ), Si-O ( $456\text{ cm}^{-1}$  and  $787\text{ cm}^{-1}$ ), and Si-O-Al ( $680\text{ cm}^{-1}$ ) [32–34]. (Figure 2A). Regarding the recognized spectrum of metakaolinite, it reflects a significant reduction in the identification bands of the –OH-bearing structural groups, demonstrating the strong de-hydroxylation and de-hydration of kaolinite during the destruction of its crystalline structure by the temperature activation step (Figure 2B). The main aluminosilicate groups were also detected clearly in the spectrum, including Si-O ( $451\text{ cm}^{-1}$  and  $778\text{ cm}^{-1}$ ), Si-O-Al ( $521\text{ cm}^{-1}$  and  $672\text{ cm}^{-1}$ ), and Si-O-Al ( $521\text{ cm}^{-1}$  and  $672\text{ cm}^{-1}$ ), but with deviated bands to lower positions signifying the impact of the amorphization process (Figure 2B).

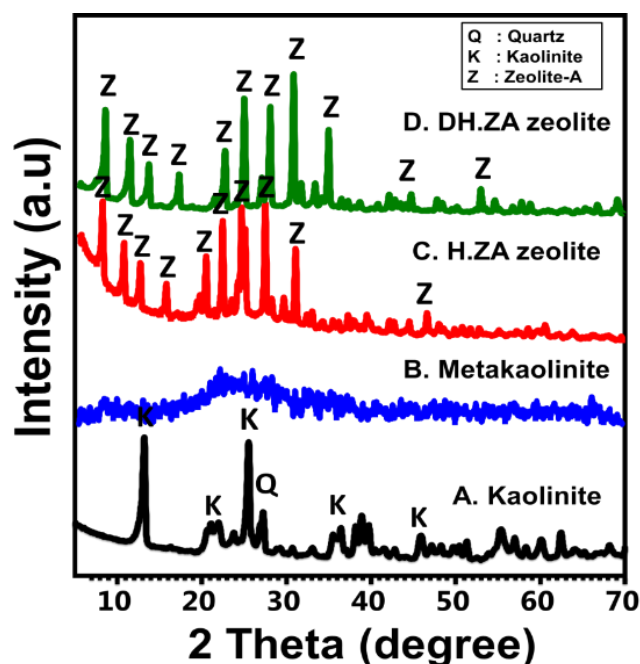


**Figure 1.** XRD patterns of raw kaolinite (A), metakaolinite (B), and synthetic zeolite-A by conventional method (hydrated zeolite) (C) and synthetic zeolite-A by alkali fusion method (dehydrated zeolite) (D).

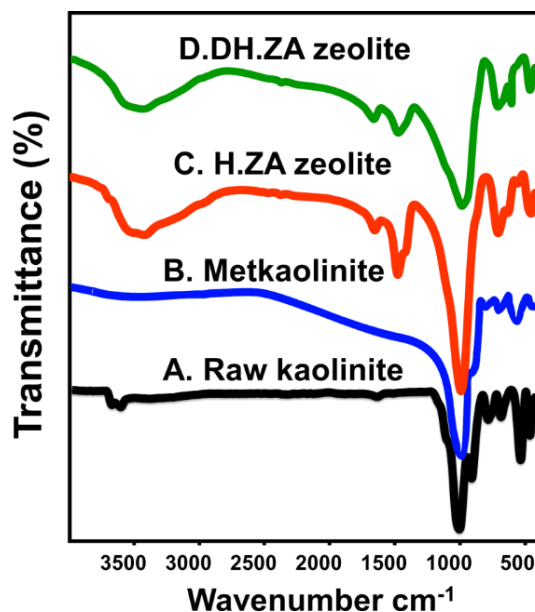


**Figure 2.** FT-IR spectra of raw kaolinite (A), metakaolinite (B), and synthetic zeolite-A by conventional method (hydrated zeolite) (C) and synthetic zeolite-A by alkali fusion method (dehydrated zeolite) (D).

Regarding the spectrum of H.ZA, it still exhibits the same bands of the structural aluminosilicate groups, but at observable deviated sites, in addition to a remarkable reduction in the commonly detected bands less than 1000 cm<sup>-1</sup> in the spectrum of kaolinite (Figure 2C). Such observations validate the structural changes from the raw phyllosilicate kaolinite into tectosilicate zeolite-A. This conversion is also associated with significant exposure for the active siloxane groups (Si-OH and Al-OH) as a result of the alkaline etching effect causing intensification in the characteristic bands of -OH (Figure 2C) [35,36]. The main detectable functional groups of H.ZA are Si-O (452.1 and 705 cm<sup>-1</sup>), Si-O-Al (555.02 and

630  $\text{cm}^{-1}$ ), Si-O-Si (990  $\text{cm}^{-1}$ ), adsorbed O-H (1652  $\text{cm}^{-1}$ ), zeolitic water (1475  $\text{cm}^{-1}$ ), Si-OH (3612  $\text{cm}^{-1}$ ), and Al-OH (3422  $\text{cm}^{-1}$ ) (Figure 2C) [37]. Regarding the spectrum of DH.ZA, it shows the same essential bands of H.ZA, but at shifted positional and low intensities, demonstrating significant structural and chemical changes that might be related to the transformation and crystallization efficiencies as well as the associated chemical substitution between the structural Al and Si in the zeolite lattice with the sodium ions (Figure 2D). The essential groups of zeolite that were identified are Si-O (460 and 707  $\text{cm}^{-1}$ ), Si-O-Al (643  $\text{cm}^{-1}$ ), Si-O-Si (984  $\text{cm}^{-1}$ ), O-H (1662  $\text{cm}^{-1}$  and 3443  $\text{cm}^{-1}$ ), and zeolitic water (1474  $\text{cm}^{-1}$ ) (Figure 2D).

### 2.1.3. XRF Analysis

To gain more details about the impact of the synthesis methods on the chemical structure of the resulting zeolite phases, the major oxides of H.ZA and DH.ZA were presented in comparison with the composition of the starting kaolinite (Table 1). The results demonstrate a significant declination in the silica content from 47.83% for raw kaolinite to 36.2% and 32.9% in H.ZA and DH.ZA, respectively (Table 1). This was also recognized for the  $\text{Al}_2\text{O}_3$  content; its percentage was reduced from 35.74% (kaolinite) to 29.2% (H.ZA) and 28.24% (DH.ZA) (Table 1). Such a declination in both  $\text{SiO}_2$  and  $\text{Al}_2\text{O}_3$  content validates their leaching for the structural units of kaolinite during its alkaline transformation reactions or the strong substitution of them with the dissolved sodium ions [36]. This assumption was supported by the detectable increment in the sodium content from 0.28% up to 13.3% and 20.2% for H.ZA and DH.ZA, respectively (Table 1). Moreover, such chemical results demonstrate the higher leaching and sodium substitution effect of the alkaline fusion method as compared to the conventional hydrothermal methods. The high alkalinity properties of the alkali fusion method and the high sodium content of the resulting zeolite (DH.ZA) validate the higher basicity properties of DH.ZA (7.73 mmol OH/g) than H.ZA (5.88 mmol OH/g), which is an essential parameter during the assessment of the products as heterogeneous catalysts (Table 1). Regarding the ion exchange capacity, the synthetic H.ZA (340 meq/100 g) exhibits a slightly higher ion exchange capacity than DH.ZA (298 meq/100 g), which might be related to the greater hydration properties of H.ZA and the existence of numerous free and exchangeable  $\text{Na}^+$  ions in the zeolitic water within its structural channels (Table 1).

**Table 1.** The chemical composition and microstructural and physicochemical properties of kaolinite, H.ZA and DH.ZA.

Chemical Properties									
Oxides	$\text{SiO}_2\%$	$\text{Al}_2\text{O}_3\%$	$\text{Fe}_2\text{O}_3\%$	$\text{MgO}\%$	$\text{CaO}\%$	$\text{TiO}_2\%$	$\text{Na}_2\text{O}\%$	$\text{K}_2\text{O}\%$	L.O.I%
Kaolinite	47.83	35.74	0.89	0.12	0.53	0.82	0.28	0.08	14
H.ZA zeolite	36.2	29.2	0.10	—	—	0.06	13.3	—	21.1
DH.ZA zeolite	32.9	28.24	0.14	—	—	0.07	20.23	—	18.4
Textural and Physicochemical Properties									
	Specific Surface Area	Total Pore Volume	Average Pore Size	Ion Exchange	Total Basicity				
Kaolinite	10 $\text{m}^2/\text{g}$	0.072 $\text{cm}^3/\text{g}$	43.2 nm	—	—				
H.ZA zeolite	423 $\text{m}^2/\text{g}$	0.382 $\text{cm}^3/\text{g}$	11.6 nm	340 meq/100 g	5.88 mmol OH/g				
DH.ZA zeolite	488 $\text{m}^2/\text{g}$	0.446 $\text{cm}^3/\text{g}$	9.2 nm	298 meq/100 g	7.73 mmol OH/g				

### 2.1.4. SEM and Microstructural Analysis

The morphological properties were studied considering the SEM images of raw kaolinite as well as the synthetic H.ZA and DH.ZA particles (Figure 3). The used kaolinite particles were detected as well-developed flakey grains of pseudo-hexagonal shape, which characterize the pure phases and high crystalline kaolinite (Figure S1). The SEM images of H.ZA as well as DH.ZA demonstrated the strong alteration of the kaolinite into well-

developed cubic grains, which is the dominant morphology of zeolite-A (Figure 3A,D). Considering the dimension of the cubic zeolite grains in the SEM images, the synthetic zeolite obtained by the fusion method (DH.ZA) exhibits a smaller grain size than the zeolite produced by the conventional method (H.ZA). This observation was supported by the determined particle size distribution of DH.ZA in comparison with H.ZA. About 95% of the DH.ZA particles exhibit grain sizes lower than 25  $\mu\text{m}$ , and 50% of them show particle sizes less than 5  $\mu\text{m}$ . On the other hand, about 95% of the prepared H.ZA particles exhibit an actual size range lower than 45  $\mu\text{m}$ , and 50% of the sample exhibits a size lower than 10  $\mu\text{m}$ . The lower particle size distribution of DH.ZA, as compared to H.ZA, induces its dispersion and homogeneity properties during its incorporation with the liquid oil and alcohol during the transesterification experiments, in addition to its impact on the surface area.

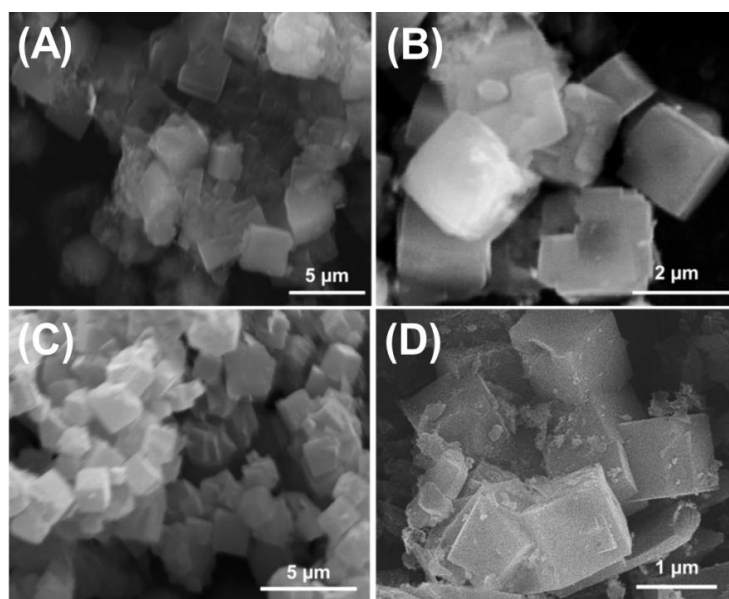


**Figure 3.** SEM images of the synthetic zeolite-A obtained by conventional method (hydrated zeolite) (A,B) and synthetic zeolite-A obtained by alkali fusion method (dehydrated zeolite) (C,D).

The differences between the two forms of synthetic LTA zeolite in their structural, morphological, and chemical properties are associated with significant changes in their textural properties. The determined surface area of H.ZA and DH.ZA is 423  $\text{m}^2/\text{g}$  and 488  $\text{m}^2/\text{g}$ , respectively (Table 1). Such values are in agreement with the obtained findings of the morphological and particle size distribution results. Additionally, the DH.ZA shows a higher pore volume (0.446  $\text{cm}^3/\text{g}$ ) and lower pore diameter (9.2 nm) than the determined values for H.ZA (0.446  $\text{cm}^3/\text{g}$  pore volume and 11.6 nm pore diameter), which are also essential factors during the evaluation of the products as catalysts (Table 1).

## 2.2. Transesterification Results

### 2.2.1. Effect of the Experimental Variables

#### Effect of Transesterification Intervals at Different Temperature

The experimental influence of the transesterification duration on the productivity of FAME yield by H.ZA (Figure 4A) and DH.ZA (Figure 4B) was followed from 20 min up to 180 min, considering the changes in the temperature of the tests from 40  $^{\circ}\text{C}$  up to 90  $^{\circ}\text{C}$  and the other parameters at fixed values (2 wt. % as catalyst load and 12:1 as methanol-to-oil molar ratio). The duration of the transesterification reactions is an essential factor in keeping the different reactants of the systems in contact with each other until achieving the best conversion efficiencies of the oil into FAME. The short intervals or the low duration of the reaction resulted in low miscibility and homogeneity between the different phases in the conversion system [38,39]. Therefore, there are poor transformation

efficiencies of the triglycerides into FAME either by H.ZA or DH.ZA at the initial stages of the conducted reactions at any adjusted temperature values (Figure 4A,B). The increment in the reaction duration resulted in regular enhancement in the miscibility properties between the reactants and, in turn, the transformation efficiencies until attending the optimum interval for each catalyst. The best durations of the performed reactions by H.ZA and DH.ZA are 140 min and 120 min, respectively, at any tested temperature values (Figure 4A,B). The tests performed for a longer duration than 140 min (H.ZA) and 120 min (DH.ZA) show a remarkable drop in the production efficiencies of FAME and its yield. This occurred commonly due to the reversible behaviors of the methanolysis reactions or the significant accelerations of the side reactions that involve the dissolution of the glycerol byproducts into the alcohol molecules [18,31].

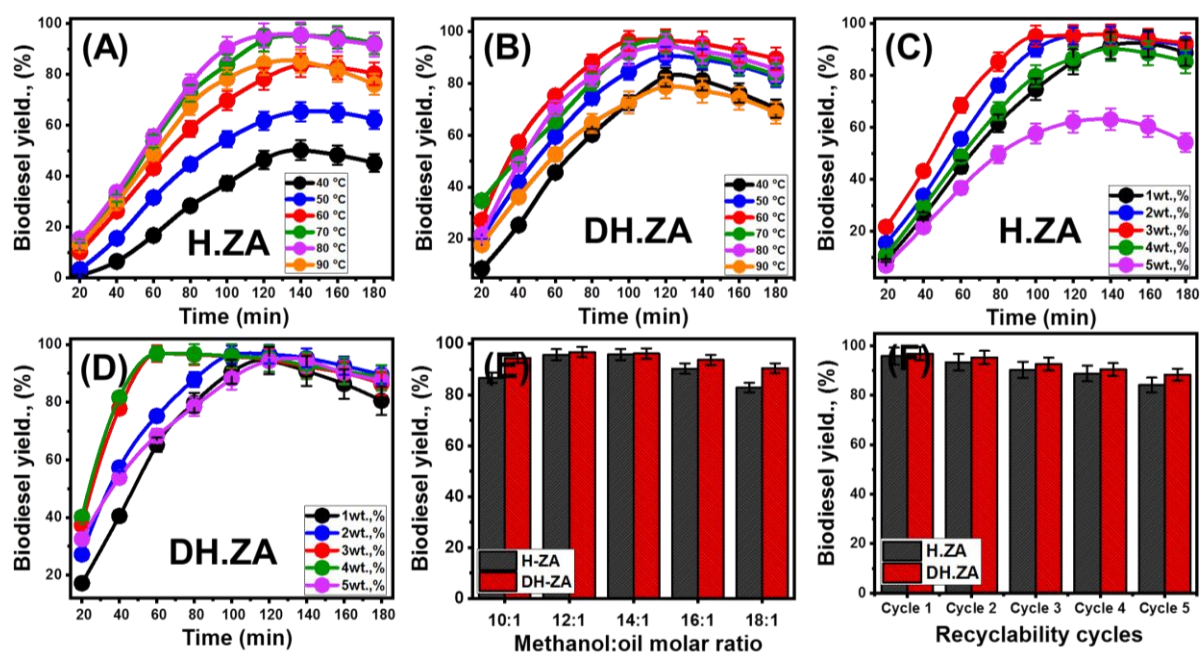


**Figure 4.** Shows the effect of the transesterification at different temperatures on the biodiesel yield obtained by H.ZA and DH.ZA (A,B), the effect of the transesterification using different loads of H.ZA and DH.ZA on the obtained biodiesel yield (C,D), the effect of the methanol-to-oil molar ratio on the obtained biodiesel yield by H.ZA and DH.ZA (E), and the recyclability properties of H.ZA and DH.ZA during the transesterification of waste cooking oil (F).

Regarding the impact of the transesterification temperature as a crucial factor during any kinetic reaction, its experimental influence was followed from 40 °C up to 90 °C in terms of the determined FAME yield using H.ZA and DH.ZA (Figure 4A,B). The increase in the temperature is associated with a strong acceleration effect on the conversion rates of FAME and an enhancement effect on the obtained yields. The best FAME yields were determined for the reactions that were performed at 80 °C (95.6%) and 60 °C (96.6%) using the H.ZA and DH.ZA catalysts, respectively, which were quite near to the determined boiling temperature value of methanol (Figure 4A,B). Within this temperature range, the conducted endothermic transesterification reactions acquired the threshold kinetic energies, which induced the effective mass transfer between the interfaces of the reactants [33,40,41]. Beyond these temperature values (80 °C (H.ZA) and 60 °C (DH.ZA)), the considerable loss of the evaporated methanol from the system negatively affects the conversion efficiency of FAME [22].

The presented FAME results and the reactions behaviors of H.ZA and DH.ZA, as a function of the transesterification duration and temperature, demonstrates considerable differences in the catalytic activities and properties of the two zeolite forms. The alkali-fused zeolite-A (DH.ZA) exhibits higher activity than the zeolite prepared by the normal

method (H.ZA) over a short duration and at low-temperature values. The higher activity of DH.ZA than H.ZA was ascribed to its high surface area and basicity in addition to its smaller particle size, which induces its miscibility and homogeneity with the other reactants within short intervals. The hydration properties of H.ZA resulted in a slight increase in the best transesterification temperature as compared to the dehydrated particles of DH.ZA.

#### Effects of the Catalyst Dosages on FAME Yield

The H.ZA and DH.ZA weight percentages during the reactions strongly affect the conversion rate and efficiency of FAME, as the presence of the catalysts at the satisfied quantities ensures the availability of the required active catalytic sites in the system [35]. The influence of H.ZA and DH.ZA loadings were assessed from 1 wt. % up to 5 wt. % considering the changes in the transesterification duration from 20 min up to 180 min and the other parameters at fixed values (12:1 as a methanol-to-oil molar ratio; 80 °C and 60 °C as reaction temperature using H.ZA and DH.ZA catalysts) (Figure 4C,D). The increment in the quantities of H.ZA and DH.ZA (1 wt. % to 3 wt. %) exhibits significant enhancement effects on the conversion rates of the oil into FAME, as well as the achieved FAME yields (Figure 4C,D). This behavior was assigned to the increase in the exposed surface area of H.ZA and DH.ZA, as well as their active catalytic sites, which in turn induce the conversion rates of the triglycerides into FAME [38,42]. (The determined FAME yield at the optimum loadings of H.ZA (95.7%) and DH.ZA (96.8%) were observed after 140 min and 60 min, respectively (Figure 4C,D). These results in terms of the transesterification duration reflect the significant accelerating impacts of the high zeolite dosages on the conversion rates, as well as the equilibration of the reactions, which can be detected clearly in the case of DH.ZA, as it is of higher catalytic activity and surface area than H.ZA. The increase in the H.ZA and DH.ZA dosages exceeding 3 wt. % causes a remarkable drop in the reaction efficiency in terms of the determined FAME yields (Figure 4C,D). This was reported as a result of the increase in the viscosity of the system negatively affecting the homogeneity and the mass transfer resistance between the three phases (zeolite, methanol, and oil) [19,40].

#### Effect of Methanol-to Oil Molar Ratio

The molar ratio of monohydric alcohol (methanol) to the triglyceride content of the spent cooking oil is an essential parameter for controlling the effect on the production efficiency of biodiesel [18,22]. Stoichiometrically, the ideal transesterification reaction to produce 3 moles of fatty acid methyl ester (FAME) and 1 mole of glycerol byproduct requires an interaction between 3 moles of methanol and 1 mole of triglyceride [38]. Considering the reversible properties of the transesterification reactions, the concentration of the used alcohol should be adjusted to values higher than the stoichiometric value to direct the process in the forward direction based on Le Chatelier's principle [33]. The experimental effect of methanol concentration in terms of its molar ratio to the oil was followed from 10:1 up to 18:1 considering the previously detected best conditions for H.ZA (120 min (time interval), 80 °C (temperature), and 3 wt. % (catalyst loading)) and DH.ZA (60 min (time interval), 60 °C (temperature), and 3 wt. % (catalyst loading)) (Figure 4E).

The determined FAME conversion efficiencies using H.ZA and DH.ZA increased at remarkable rates with the experimental increase in the methanol contents, which corresponded to the molar ratios of 14:1 (95.8% FAME yield) and 12:1 (96.8% FAME yield), respectively (Figure 4E). This was assigned to the reducing effect of the excess in the methanol content on the viscosity and immiscibility properties between the reactants as well as the mass transfer resistance [6,43]. Additionally, the excess in the methanol concentration significantly accelerates the interaction between the zeolite-A particles and the present triglycerides up to a certain extent [33]. Increasing the molar ratios of methanol above the previously detected optimum values (12:1 (H.ZA) and 14:1 (DH.ZA)) resulted in adverse effects on the FAME production efficiencies by H.ZA and DH.ZA (Figure 4E). This behavior was assigned to the dissolution of the glycerol molecules in the excess methanol, which negatively affects the proper separation of the glycerol-biodiesel phase and the reaction



balance, directing to the reversible direction [21,38]. Additionally, the excess unreacted methanol molecules can deactivate the active catalytic sites of zeolite-A catalysts and might convert into emulsifier centers after the inversion of their polar groups, which reduces the performance of H.ZA and DH.ZA transesterification systems [22].

#### Recyclability of H.ZA and DH.ZA Catalysts

The stability and recyclability properties of H.ZA and DH.ZA as heterogeneous catalysts are essential factors to evaluate the sustainable values of the studied materials during the commercial- and industrial-scale production of biodiesel. The incorporated H.ZA and DH.ZA particles in each transesterification test were separated from the liquid phases by centrifugation and washed for five runs with methanol as an organic regeneration reagent with a significant dissolving effect on the accumulated glycerol and fatty acids on their surfaces. The washed particles of H.ZA and DH.ZA were subsequently dried gently within a digital drier for 12 h at 80 °C and reused in another cycle of the transesterification reaction. The recyclability properties of the two forms of zeolite-A during the studied transesterification processes of waste cooking oil were assessed considering the previously estimated best conditions of H.ZA (120 min (time interval), 80 °C (temperature), 14:1 (methanol/oil ratio), and 3 wt. % (catalyst loading)) and DH.ZA (60 min (time interval), 60 °C (temperature), 12:1 (methanol/oil ratio), and 3 wt. % (catalyst loading)) (Figure 4F).

The recognized results signify the remarkable stability of both H.ZA and DH.ZA as solid multi-phase or heterogeneous catalysts to be reused effectively five times in the production of biodiesel from waste cooking oil feedstock. The reuse of H.ZA particles resulted in biodiesel yields higher than 90.3% after three recyclability cycles and higher than 84% after the studied five recyclability cycles (Figure 4F). Regarding the stability of DH.ZA, the reuse of its particles as catalysts resulted in biodiesel yields of more than 92.5% after three recyclability cycles and more than 88% after five recyclability cycles (Figure 4F). Considering the determined yields, the synthetic DH.ZA also shows higher recyclability and stability than H.ZA, which can be ascribed to the previously reported differences in their textural and chemical properties. Regarding the detected decline in the activities of the H.ZA and DH.ZA catalysts in terms of the achieved yields when increasing the assessed reusability cycles, this was ascribed to the predicted leaching of the exchangeable Na<sup>+</sup> ions during the washing steps [44,45]. Additionally, there were expected deactivation impacts of the remaining glycerol molecules on the active functional groups as catalytic centers on the surfaces of H.ZA and DH.ZA [18].

#### 2.2.2. Physical and Safety Properties of the Obtained Biodiesel

The physical properties of the biodiesel samples obtained from H.ZA and DH.ZA were determined and compared with the recommended values for suitable biofuels according to both ASTM D-6751 and EN 14214 international standards (Table 2). The measured values of the density and viscosity of the two samples are within the accepted ranges according to the two standards, which qualify the two products to be applied as fuels. Additionally, the measured values of the cetane index are higher than 45, which signifies the high qualification of the samples to be used as fuels, considering the ignition delay time and combustion quality. Moreover, this value reflects the remarkable safety properties of the obtained samples, indicating that they can be used safely in engines [38]. The measured values of both the flashpoint and calorific value qualify the two products to be used as safe fuels during the different handling and transport processes, which is supported by the determined low values of the pour point and cloud point (Table 2).

**Table 2.** The physical properties of the biodiesel samples obtained from H.ZA and DH.ZA catalysts.

Contents	Unit	ASTM D-6751	EN 14214	H.ZA	DH.ZA
Viscosity	mm <sup>2</sup> /s	1.9–6	3.5–5	3.61	3.66
Moisture content	Wt.(%)	<0.05	<0.05	0.047	0.038
Flash point	°C	>93	>120	128.6	133.2
Calorific value	MJ/kg	—	>32.9	43.3	46.5
Cloud point	°C	−3 to 15	—	6.3	6.7
Pour point	pp	−5 to 10	—	5.5	5.8
Cetane number	—	≥47	≥51	60.4	66.3
Density	g/cm <sup>3</sup>	0.82–0.9	0.86–0.9	0.866	0.871
Acid value	Mg/KOH/g	≤0.5	≤0.5	0.38	0.34
Iodine value	—	—	≤120	108.5	110.3

### 2.2.3. The Suggested Mechanism

Based on the obtained FT-IR spectra of the fresh (Figure 2) and spent (Figure 5) H.ZA and DH.ZA particles after the transesterification tests, the transformation mechanism of the oil triglycerides in the presence of these particles as catalysts can be described (Figure 6). The detection of new bands related to a sCH<sub>2</sub> aliphatic group and ester carbonyl groups in the spectra of the spent zeolite particles in comparison with the fresh particles suggested significant adsorption of the present triglycerides by both H.ZA and DH.ZA. In step I, the basic NaO bond interacts with triglyceride, as shown in Figure 5. Many researchers have reported that an interaction takes place between methanol and active species to produce methoxide ions. Herein, sodium methoxide was not detected. Additionally, the pH of methanol is higher than when spent; hence, it is more feasible for triglyceride to interact with basic NaO. The pH of methanol and feedstocks were primarily investigated [33]. The FT-IR of the used catalyst indicates the presence of a CH<sub>2</sub> (2900 cm<sup>−1</sup>) aliphatic group and an ester carbonyl functionality (1300 cm<sup>−1</sup>) for the symmetric stretching of C-O-C, which also strongly supports the formation of a bond between NaO and CH<sub>2</sub> aliphatic [46,47]. Step II indicates the surface interaction between methyl alcohol and adsorbed triglyceride at the active surface of the catalyst. The methoxide (CH<sub>3</sub>O<sup>−</sup>) substitutes the position of O in NaO to form fatty acid methyl ester, which is rapidly generated from the catalyst's active surface. In the final step, glycerol molecules are formed because of the capturing of hydrogen ions by the glycerol backbone and are finally desorbed from the surfaces of the zeolite particles, which makes their active sites free for another cycle of triglyceride interactions (Figure 6) [33].

Considering the previous mechanistic steps, the synthetic dehydrated form of zeolite-A (DH.ZA) exhibits enhanced physicochemical properties capable of accelerating the transesterification reactions as compared to the hydrated form, reflecting a significant impact of the synthesis processes on the catalytic activity of zeolite-A. The synthetic DH.ZA particles exhibit higher surface area, sodium content, and total basicity in addition to their smaller particle size than the H.ZA particles. The previous factors induce the mixing and dispersion properties of DH.ZA particles within the oil sample. Moreover, the high surface areas of DH.ZA particles are of a significant enhancement effect during the adsorption of triglyceride molecules.

### 2.2.4. Kinetics and Thermodynamics

The kinetic and thermodynamic functions of the transesterification process of waste cooking oil by DH.ZA and H.ZA were evaluated according to the procedures presented in Section 2. The estimated parameters are the reaction rate constant and activation energy, in addition to the thermodynamic parameters, considering the different tested temperature values. The addressed thermodynamic parameters involved the entropy of activation, enthalpy of activation, and Gibb's free energy.

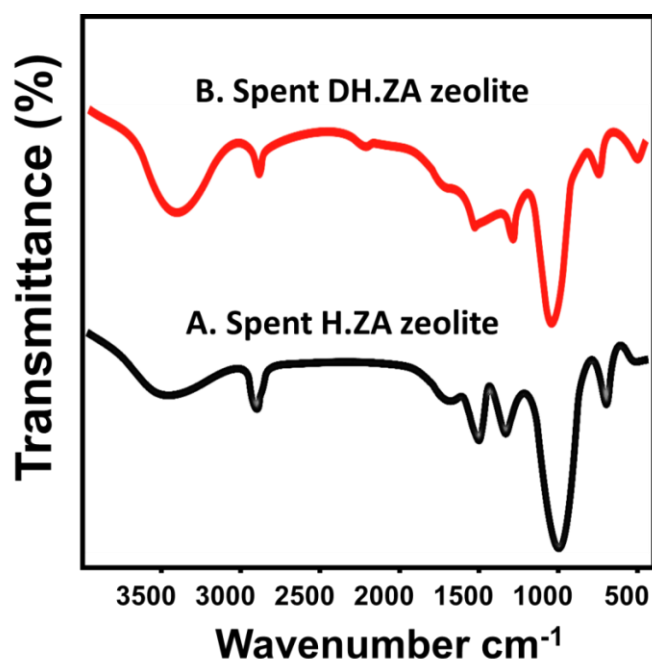


Figure 5. FT-IR spectra of spent H.ZA and DH.ZA after the transesterification reactions.

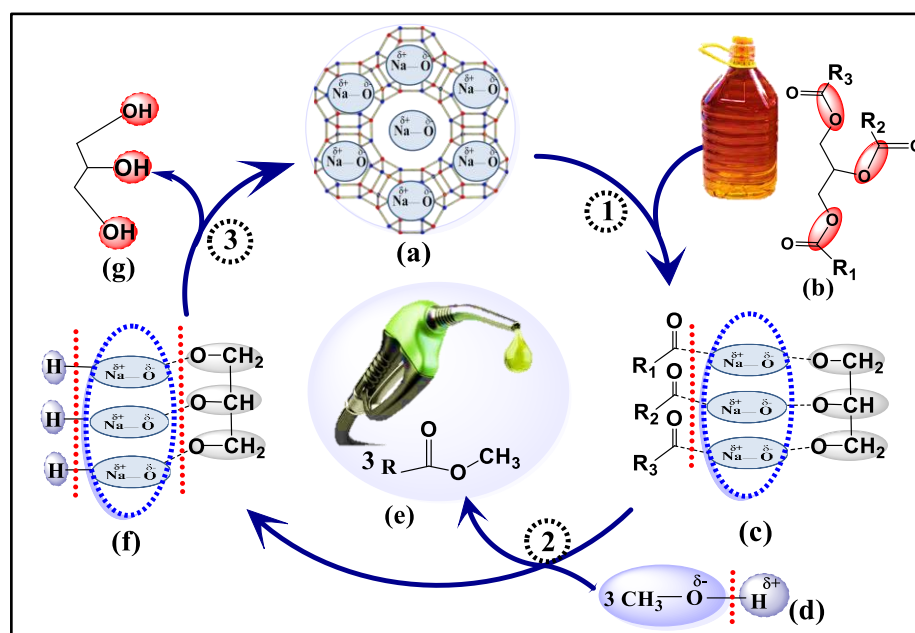
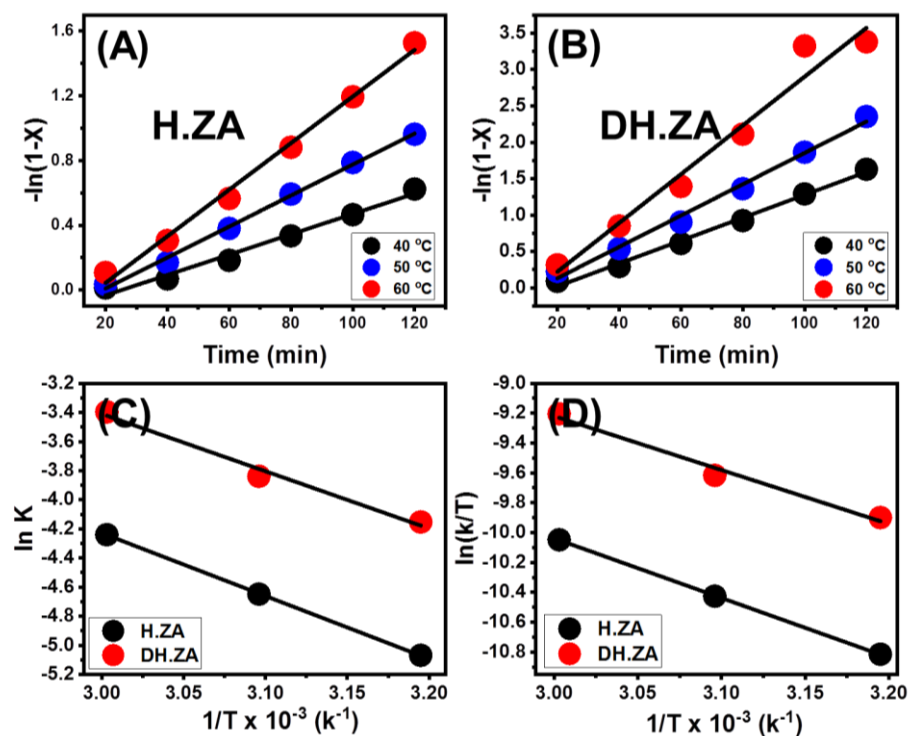


Figure 6. Schematic diagram for the transesterification mechanism of waste cooking oil over the synthetic zeolite-A particles.

#### Determination of the Rate Constant Values

The rate constant ( $k_c$ ) values during the transesterification reactions by DH.ZA and H.ZA were obtained as fitting parameters for the linear regression plotting of  $-\ln(1 - X)$  versus the experimental transesterification time intervals (Figure 7A,B; Table 3). This was performed considering the change in the adjusted temperature (40, 50 and 60 °C), the FAME conversion intervals from 20 min up to 120 min, and the previously determined best-operating conditions of catalyst loading and the methanol ratio. Based on the determination coefficient values ( $R^2 > 0.95$ ) of the plotted kinetic graphs, the methanolysis and the transesterification of waste cooking oil over DH.ZA and H.ZA occurred according to the kinetic properties of the pseudo-first-order kinetic model. Therefore, the adsorption-surface

reaction-desorption processes are the essential operating mechanisms that control the transesterification of waste cooking oil by both DH.ZA and H.ZA, which is in agreement with the suggested mechanism based on the FT-IR findings [43,48]. Moreover, the increase in the rate constant with temperature and their higher values during the applications of DH.ZA as compared to H.ZA is in agreement with the experimental findings regarding the impact of temperature and the higher catalytic activity of DH.ZA than H.ZA.



**Figure 7.** Fitting of the transesterification results by H.ZA and DH.ZA with the pseudo-first-order kinetic model (A,B), fitting of the transesterification results with Arrhenius equation (C), and fitting of the transesterification results with Eyring–Polanyi equation (D).

**Table 3.** The values of the determined determination coefficient and rate constant values of the transesterification reactions by both H.ZA and DH.ZA as fitting parameters of pseudo-first-order kinetic model.

Catalyst	Temperature	Rate Constant (k (min <sup>-1</sup> ))	Determination Coefficient (R <sup>2</sup> )
H.ZA	40 °C	0.00629	0.9784
	50 °C	0.00958	0.9961
	60 °C	0.01441	0.9911
DH.ZA	40 °C	0.01572	0.9919
	50 °C	0.02152	0.9900
	60 °C	0.03351	0.9588

#### The Reaction Activation Energy and Pre-Exponential Values

The activation energy values of the reactions that occurred during the transesterification processes utilizing the H.ZA and DH.ZA particles were obtained according to the Arrhenius equation as a fitting parameter for the linear regression plotting of  $\ln(K_c)$  versus  $1/T$  (Figure 7C; Table 4). The recognized values of activation energies using both H.ZA (35.9 kJ·mol<sup>-1</sup>) and DH.ZA (32.714 kJ·mol<sup>-1</sup>) are 35.9 kJ·mol<sup>-1</sup> and 32.714 kJ·mol<sup>-1</sup>, respectively, while the estimated values of the pre-exponential factor are 6179.66 min<sup>-1</sup> (H.ZA) and 4421 min<sup>-1</sup> (DH.ZA). The lower value of activation energy resulted in a lower energy

barrier, while higher values of the frequency factor or pre-exponential factors reflected the increased collisions between reactants and active sites of the catalyst, which accelerated the methylation of the triglycerides [12,48]. Despite the fact that the pre-exponential factor of DH.ZA was somewhat lower than that of H.ZA, the distinct low activation energy value of DH.ZA resulted in a greater transesterification rate.

**Table 4.** The activation energy and pre-exponential values of the transesterification reactions by both H.ZA and DH.ZA according to the Arrhenius equation.

Parameters	H.ZA	DH.ZA
Slope	−4.31938	−3.93487
Intercept	8.72902	8.39413
Determination coefficient ( $R^2$ )	0.99983	0.97338
Activation energy ( $\Delta E^*$ ) ( $\text{kJ}\cdot\text{mol}^{-1}$ )	35.9	32.714
Pre-exponential value (A) ( $\text{min}^{-1}$ )	6179.66	4421.03

#### The Thermodynamic Functions (Enthalpy, Entropy, and Gibb's Free Energy)

The essential thermodynamic functions for the transesterification reactions that occurred by H.ZA and DH.ZA were estimated based on the Eyring–Polanyi equation as fitting parameters for the linear regression plotting of  $\ln(k_c/T)$  versus  $1/T$  (Figure 7D; Table 5). The recognized positive signs of both the enthalpy of activation ( $\Delta H^*$ ) ( $33.23 \text{ kJ}\cdot\text{mol}^{-1}$  (H.ZA) and  $30.03 \text{ kJ}\cdot\text{mol}^{-1}$  (DH.ZA)) and Gibb's free energy ( $\Delta G^*$ ) ( $65.164 \text{ kJ}\cdot\text{mol}^{-1}$  (H.ZA) and  $65.268 \text{ kJ}\cdot\text{mol}^{-1}$  (DH.ZA)) demonstrate the endothermic and spontaneous properties of the transesterification reactions of waste cooking oil that occurred with both H.ZA and DH.ZA. This was supported by estimating the values of the entropy of the activation with negative signs either for H.ZA ( $-195.59 \text{ J}\cdot\text{K}^{-1}\cdot\text{mol}^{-1}$ ) or DH.ZA ( $-195.91 \text{ J}\cdot\text{K}^{-1}\cdot\text{mol}^{-1}$ ), which also suggested a decrease in the randomness properties of the reactions.

**Table 5.** Evaluation of thermodynamic parameters from Eyring–Polanyi plot:  $\ln(K_C/T)$  vs.  $1/T \times 10^{-3}$ .

Thermodynamic Parameters	H.ZA	DH.ZA
Slope	−3.99664	−3.61213
Intercept	1.95184	1.61696
$R^2$	0.99983	0.96888
Enthalpy of activation ( $\Delta H^*$ ) ( $\text{kJ}\cdot\text{mol}^{-1}$ )	33.23	30.03
Entropy of activation ( $\Delta S^*$ ) ( $\text{J}\cdot\text{K}^{-1}\cdot\text{mol}^{-1}$ )	−195.59	−195.91
Gibb's free energy of activation ( $\Delta G^*$ ) ( $\text{kJ}\cdot\text{mol}^{-1}$ )		
40 °C	61.252	61.349
50 °C	63.208	63.308
60 °C	65.164	65.268

#### 2.2.5. Comparison Study

The catalytic activities of the synthetic H.ZA and DH.ZA particles from Egyptian kaolinite during the transesterification of waste cooking oil were compared with other studied catalysts in the literature, considering the experimental conditions (Table 6). The presented values reflect the higher activities of the synthetic zeolite-A produced from Egyptian kaolinite than most of the assessed catalysts in the literature, including synthetic apatite, nickel oxide-based catalysts, CaO, cesium-modified silica, CaO/SiO<sub>2</sub> composite, and Kettle limescale (Table 6). Additionally, the presented comparison signifies the significant positive impact of the alkali fusion method as a synthesis method of zeolite-A (DH.ZA) on its textural and catalytic activity as a catalyst during the transesterification of spent vegetable oils.

**Table 6.** Comparison between the obtained biodiesel yield using the H.ZA and DH.ZA catalysts and other catalysts in literature.

Catalyst	Time	Temperature (°C)	Methanol/Oil Ratio	Dosage (wt. %)	Yield (%)	References
Ba-Zeolite	2 h	65.38	12:1	3	93.17	[49]
CaO/zeolite	238.8 min	69.1	9.7:1	2.1	93.7	[50]
CaO/Zeo-CTAB	4 h	65	5:1	4	89	[51]
FAU zeolite	4 h	65	9:1	5	91.6	[3]
Na <sub>2</sub> SiO <sub>3</sub>	12 h	28	12:1	5	96	[12]
CaO/SiO <sub>2</sub>	3 h	65	21:1	11	90.2	[52]
Kettle limescale	15 min	61.7	3:1.7	8.9	93.4	[53]
Zeolite Na-X	8 h	65	6:1	3	83.5	[54]
CaO	3 h	65	20:1	5	95	[55]
Cesium-modified silica	3 h	65	20:1	3	90	[56]
Coconut coir husk	3 h	130	12:1	10	89.8	[57]
Diatomite/CaO/MgO	2 h	90	15:1	6	96.4	[6]
Ni/NiO@ Diatomite	117 min	63.7	11.6:1	4	93.2	[19]
H.ZA	120 min	80	14:1	3	95.8	This study
DH.ZA	60 min	60	12:1	3	96.8	This study

### 3. Experimental Work

#### 3.1. Materials

The kaolinite precursor used during the synthesis of the two forms of zeolite-A was obtained from the Central Metallurgical Research and Development Institute (CMRDI), Egypt. NaOH pellets (97% purity, Alfa Aesar) were used during the synthesis of the two forms of zeolite-A. The waste cooking oil sample that was used during the transesterification reactions is a commercial sample representing a mixture from different local restaurants and including different species of cooking and vegetable oils. The chemical composition of the studied waste cooking oil sample is presented in Table S1.

#### 3.2. Synthesis of the Zeolite-A Catalysts

##### 3.2.1. Synthesis of Zeolite-A by Conventional Hydrothermal Method

This method firstly involved the thermal activation of crystalline kaolinite for 5 h at 650 °C into amorphous and reactive metakaolinite. After that, the produced metakaolinite powder was mixed with NaOH pellets within 50 mL of distilled water at an adjusted weight ratio of 1(metakaolinite (3 g)):2 (NaOH (6 g)). The mixture was left overnight under continuous stirring to form aluminosilicate gel and then was transferred into a Parr reactor of a Teflon-lined stainless steel autoclave, which was heated for 8 h at 100 °C using a digital muffle furnace. After the hydrothermal treatment step, the synthetic zeolite was obtained by centrifugation, washed and neutralized over numerous runs with distilled water, dried for 10 h at 65 °C, and labeled as hydrated zeolite-A (H.ZA).

##### 3.2.2. Synthesis of Zeolite-A by the Alkali Fusion Method

This method involved the fusion of the kaolinite powder (6 g) in the presence of NaOH solid pellets (7.2 g) for 5 h at 650 °C. The alkali/kaolinite fused product or mixture was ground after that to be within the size range from 100 µm up to 350 µm. Then, the fused alkali/kaolinite fractions were dispersed within 100 mL of distilled water for 120 min at an adjusted temperature of 70 °C using a magnetic stirrer at a fixed stirring speed of 500 rpm. After that, the mixture was transferred into the Parr reactor of a Teflon-lined stainless steel autoclave, which was heated for 4 h at 90 °C using a digital muffle furnace. By the end of the hydrothermal step, the synthetic zeolite was obtained by centrifugation, washed and neutralized over numerous runs with distilled water, dried for 10 h at 65 °C, and labeled as dehydrated zeolite-A (DH.ZA).

### 3.3. Characterization of the Catalysts

The crystallinity properties of both H.ZA and DH.ZA were studied considering their X-ray diffraction patterns (XRD), which were determined by an X-ray diffractometer (PANalytical, Empyrean) with Cu-K $\alpha$  radiation. The average crystallite size was determined according to the Scherrer equation ( $D = 0.9\lambda/W \cos\theta$ ), where  $W$  is the full width at half maximum in radians,  $\theta$  is Bragg's angle, and  $\lambda$  is the X-ray wavelength (CuK $\alpha = 0.15405$  nm). The changes in the morphology in terms of the synthesis technique and the conversion methods were followed based on the SEM images of the materials using a scanning electron microscope (Gemini-Zeiss, Ultra 55). The functional chemical groups were assessed based on the FT-IR spectra of raw kaolinite, H.ZA, and DH.ZA by a Fourier transform infrared spectrometer (FTIR-8400S) within a detection range from 400 cm $^{-1}$  to 4000 cm $^{-1}$ . The basicity values of H.ZA and DH.ZA were measured according to the reported procedure by [31]. A total of 0.5 of the synthetic zeolite phases were homogenized within about 50 mL of distilled water in the presence of diluted HCl (0.1 M) for 24 h. After that, 25 mL of the obtained solutions were titrated with NaOH solution (0.1 M) in the presence of phenolphthalein as a chemical indicator. The ion exchange capacities of H.ZA and DH.ZA were measured by the BaCl $_2$  technique based on the reported procedures by [32]. The surface area and the porosity of the two zeolite forms were determined by the Beckman Coulter surface area analyzer (SA3100 type) considering their N $_2$  adsorption/desorption isotherm curves considering the Brunauer–Emmett–Teller method (BET) and the Barrett–Joyner–Halenda method (BJH), respectively, during the analysis of the data.

### 3.4. Transesterification System

Stoichiometrically, the transesterification process of each one mol of triglyceride in the presence of three mol of methanol resulted in one mol of pure glycerol and 3 mol of fatty acid methyl ester (FAME). Considering the previous stoichiometrical consideration, the transesterification of the studied spent oil was accomplished by considering different values of the incorporated reactants to attend to the appropriate ratios. All the reactions were executed using a 150 mL Teflon autoclave as a reactor supplied with a magnetic stirrer and a numerical hot plate to control the mixing efficiencies and the temperature at specific values. The crucial variables which have been assessed during the transesterification of spent cooking oil over the two forms of synthetic zeolite-A (hydrated zeolite-Na-A (H.ZA) and dehydrated zeolite-Na-A (DH.ZA) are the reaction duration, methanol concentration, and temperature, while also considering the interaction between these parameters. The conducted experimental procedures involved the filtration and heating of 40 g of spent cooking oil (70 °C for 30 min) to verify the purification of the sample from any tough suspensions or water molecules. This was followed by blending the spent cooking oil with the solid particles of H.ZA and DH.ZA for 10 min with a systematic increase in the applied temperature up to the selected value of the transesterification experiment. This was followed by the addition of the methanol at the selected molar ratio for a specific time interval. By attending the end of the experiment intervals, the solid particles of the two zeolite forms were separated carefully by centrifugation, and the liquid constituents were poured directly into glass separating funnels. The liquid samples had been left overnight to certify the whole separation of the propane 1,2,3 tri-alcohol as byproducts from the obtained methyl esters (biodiesel) at the bottommost of the separating funnel. Then, the separated biodiesel was handled by an additional treatment step involving gentle heating at 70 °C for about 4 h to ensure the whole evaporation of the loose methanol molecules. The percentages, as well as the types of the formed FAME, were estimated based on the GC-mass analysis using a gas chromatography-mass spectroscopy (GC-Mass) instrument (Agilent 7890A), and the calculated yield was obtained considering Equation (1).

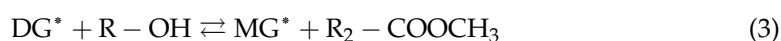
$$\text{Biodiesel yield (\%)} = \frac{\text{weight of biodiesel} \times \% \text{ FAME}}{\text{weight of triglycerides}} \times 100 \quad (1)$$

### 3.5. Analysis of the FAME Samples

The inspection of the samples was performed using an Agilent-7890A gas chromatography-mass spectroscopy (GC-Mass) instrument. The determination steps involved the controlled dilution of the extracted FAME products using normal hexane as a solvent. The quantities of the FAME in the obtained samples were measured depending on the Agilent-7890A series gas-chromatograph system coupled with a system of split/splitless injection, a flame ionization detector, and a capillary column DB WAX with dimensions of  $30\text{ m} \times 0.25\text{ mm} \times 0.25\text{ }\mu\text{m}$  that contained hydrogen gas as a carrier with a split ratio of 100:1. The temperature of both the detector and injector was maintained at  $280\text{ }^\circ\text{C}$  during the analysis of the obtained biodiesel samples. The operating temperature of the oven was adjusted firstly to  $120\text{ }^\circ\text{C}$ , and after that, the value was increased gradually to  $260\text{ }^\circ\text{C}$  as the highest temperature. The formed FAME was determined by the fixed injection of the FAME molecules using methyl heptadecanoate ( $1\text{ }\mu\text{L}$ ) as the measuring analytical internal standard.

### 3.6. Kinetics and Thermodynamics

The kinetic properties of both H.ZA and DH.ZA as basic catalysts during methanolysis of triglycerides depends on the general assumption that describes the overall transesterification chemical reaction according to three consecutive reversible reactions (Equations (2)–(4)) [33].



Hence, the overall transesterification reaction can be summarized according to Equation (5). Stoichiometrically, each mol of triglyceride (TG), diglyceride ( $\text{DG}^*$ ), and monoglyceride ( $\text{MG}^*$ ) interact with one mol of alcohol (R-OH) to form 1 mol of pure glycerol (GL) and 3 mol of fatty acid methyl ester ( $\text{R}_3\text{-COOCH}_3$ ) [20]. Based on the mechanistic steps that were reported in the literature, the production of FAME was divided into three main steps: (1) the adsorption of triglycerides on the catalyst's surface, (2) the surface reaction, and (3) the desorption of glycerol [22].



#### 3.6.1. Adsorption of Triglyceride on Catalyst Surface

The methanolysis of triglyceride that occurred on the surfaces of H.ZA and DH.ZA as catalysts resulted in the formation of several species of fatty acid methyl esters at a higher molarity of methanol-to-oil than the triglycerides. This involved, firstly, the effective adsorption of TG on the surfaces of the catalysts (Equation (6)), where the used symbols of S and TG.S refer to the unoccupied sites on the surfaces of H.ZA and DH.ZA as catalysts and the adsorbed triglyceride molecules, respectively. Moreover, the rate law of this reaction can be expressed by Equation (7).



$$r_{\text{ad}} = K_a[\text{TG}][\text{S}] - (K_{-a}[\text{TG.S}]) \quad (7)$$

#### 3.6.2. Surface Reaction

The adsorbed triglyceride molecules (TG.S) react with the excess amounts of the incorporated alcohol, producing fatty acid methyl ester and glycerol as a byproduct. The resulting glycerol tends to be adsorbed by the present active sites on the surfaces of H.ZA and DH.ZA, which are associated with the facile release of the biodiesel molecules according



to Equation (8), where the used symbol of GL.S refers to the adsorbed glycerol molecules. Moreover, the rate of the occurred surface reaction can be expressed in Equation (9) [33].



$$r_s = K_s[R-OH][TG.S] - (K_{-s}[GL.S][R-COOCH_3]) \quad (9)$$

### 3.6.3. Desorption

The desorption reaction of the formed 1, 2, 3 tri-propanol (glycerol) can be illustrated based on Equation (10), and the rate of the desorption reaction can be expressed by Equation (11).



$$r_d = K_d[GL.S] - (K_{-d}[GL][S]) \quad (11)$$

Considering the previous assumptions and findings, the general equation of the three steps can be summarized in Equation (12), in which  $S_{total}$  donates the total surface concentration as the sum of vacant surface (S), adsorbed triglycerides concentrations TG.S and adsorbed glyceryl alcohol concentration GL.S. According to this equation (Equation (12)), the surface reaction rate can be expressed after replacing the values of S, TG.S, and GL.S by  $S_{total}$  as in Equation (13). Considering the desorption of 1, 2, 3 tri-propanol at a higher rate than the adsorption rate, the values of both  $K_a [TG]$  and  $[GL]/K_d$  at zero, the existence of methanol [R-OH] at higher concentrations than the present triglyceride, which induce the neglecting of the alcohol content, and the constant value of  $S_{total}$  for the given catalyst, the final form of the rate equation of the general transesterification reactions can be expressed by Equation (14), in which the  $K_c$  symbol identifies the final rate constant of the reaction and can be calculated from Equation (15).

$$[S_{total}] = [S] + [TG.S] + [GL.S] \quad (12)$$

$$r_s = K_a \cdot K_s [S_{total}] ([TG][R-OH] - [GL][R-COOCH_3]/K_c) / (1 + K_a [TG] + [GL]/K_d) \quad (13)$$

$$r_s = d[TG]/dt = K_c [TG] \quad (14)$$

$$K_c = K_a \times K_s \times [R-OH] \times [S_{total}] \quad (15)$$

Considering the changes in the TG from the start of the transesterification process  $[TG]_0$  to certain time intervals  $[TG]_t$ , the equation can be written as in Equation (16). From the mass balance, the methyl ester conversion ( $X_{(R-COOCH_3)}$ ) can be obtained according to Equation (17) and, consequently Equation (18).

$$-\ln([TG]_t/[TG]_0) = K_c \times t \quad (16)$$

$$X_{(R-COOCH_3)} = 1 - ([TG]_t/[TG]_0) \quad (17)$$

$$[TG]_t = [TG]_0 \times (1 - X_{(R-COOCH_3)}) \quad (18)$$

Considering the integration of the rate equation in terms of X, the final equation can be expressed in Equation (19). Therefore, the rate of the transesterification processes depends only on the concentrations of the present triglyceride (TG), and in turn, the occurred reactions follow the kinetic assumption of the pseudo-first-order kinetic model [22].

$$-\ln(1 - X_{(R-COOCH_3)}) = K_c \times t \quad (19)$$

### 3.7. The Activation Energy ( $E_a$ )

The activation energy of the transesterification processes is ascertained using the Arrhenius equation (Equation (20)). The  $E_a$  value can be obtained as a fitting parameter for the linear regression plotting of  $\ln(K_c)$  against the reciprocal of the activation temperature

(1/T). The activation energy  $E_a$  and pre-exponential value ( $\ln(A)$ ) can be determined from the slope and intercept values, respectively.

$$K_c = A \exp(-E_a/RT) \quad (20)$$

### 3.8. The Thermodynamic Parameters

The thermodynamic functions of the transesterification reactions that occurred by H.ZA and DH.ZA as basic catalysts were obtained according to the Eyring–Polanyi equation (Equation (21)), where the presented  $K$ ,  $R$ ,  $h$ , and  $K_b$  symbols signify the rate constant, the universal gas constant, Planck constant ( $6.626176 \times 10^{-34}$  Js), and Boltzmann constant ( $1.3806 \times 10^{-23}$  K<sup>-1</sup>), respectively. The changes in both enthalpy ( $\Delta H^*$ ) and entropy ( $\Delta S^*$ ) were determined as fitting parameters from the slope ( $-H^*/\Delta RT$ ) and intercept, respectively, of the linear regression plot of  $\ln(K/T)$  vs.  $(1/T)$ . However, the Gibbs free energy values were ascertained according to Equation (22).

$$\ln(K/T) = -(\Delta H^*/RT) + \ln(K_b/h) + (\Delta S^*/R) \quad (21)$$

$$\Delta G^* = \Delta H^* - T\Delta S^* \quad (22)$$

## 4. Conclusions

Two forms of zeolite-A (hydrated (H.ZA) and dehydrated (DH.ZA)) were synthesized by different methods and characterized as catalysts during the transesterification processes of waste oil. The DH.ZA form exhibits enhanced physicochemical properties (488 m<sup>2</sup>/g surface area and 7.73 mmol OH/g total basicity) and catalytic activities as compared to H.ZA (423 m<sup>2</sup>/g surface area and 5.88 mmol OH/g total basicity). The obtained yields by DH.ZA (96.8%) and H.ZA (95.8%) were recognized after 60 min (60 °C) and 120 min (80 °C) under mild conditions. The transesterification reactions utilizing the forms of zeolite-A involved adsorption, surface reaction, and desorption processes, which were supported by the kinetic findings of the studied pseudo-first-order model. The determined activation energies and thermodynamic parameters (enthalpy, Gibb's free energy, and entropy) validate the spontaneous and endothermic properties of H.ZA and DH.ZA transesterification systems and their efficiencies to be applied at low-temperature conditions. Both H.ZA and DH.ZA are of significant stability, and the biodiesel samples obtained by them are of acceptable technical properties according to recommended international standards.

**Supplementary Materials:** The following supporting information can be downloaded at: <https://www.mdpi.com/article/10.3390/catal13010030/s1>, Table S1: the Fatty acid content and physical properties of the inspected waste cooking oil. Figure S1: SEM image of the used raw kaolinite during the synthesis of zeolite-A.

**Author Contributions:** Conceptualization, M.R.A., S.B., J.S.A. and M.A.S.; methodology, M.A.S., W.A.Z. and S.I.O.; Software, M.A.S., A.A.A. and W.A.Z.; validation, M.R.A., S.B., J.S.A., A.A.A. and S.I.O.; formal analysis, M.A.S., A.A.A., S.I.O. and S.A.A.; investigation, M.R.A., S.B., J.S.A. and A.A.A.; resources, A.A.A., M.A.S., W.A.Z. and S.I.O.; data curation, M.R.A., M.A.S., W.A.Z. and S.I.O.; writing—original draft preparation, M.R.A., M.A.S., S.I.O., A.A.A., S.B., J.S.A., W.A.Z. and S.A.A.; writing—review and editing, M.R.A., M.A.S., S.I.O., A.A.A., S.B., W.A.Z. and S.A.A.; visualization, M.R.A., M.A.S. and S.B.; supervision, M.R.A., S.B., A.A.A. and S.A.A.; project administration, S.I.O., M.R.A., J.S.A. and A.A.A.; funding acquisition, S.I.O. and J.S.A. All authors have read and agreed to the published version of the manuscript.

**Funding:** This research was funded by [King Saud University] grant number [RSP2023R149] and Princess Nourah bint Abdulrahman University grant number [PNURSP2022R5].

**Data Availability Statement:** Data are available upon reasonable, by the corresponding authors.

**Acknowledgments:** The authors acknowledge the Researchers Supporting Project number (RSP2023R149), King Saud University, Riyadh, Saudi Arabia. Additionally, the authors acknowledge Princess Nourah bint Abdulrahman University Researchers Supporting Project number (PNURSP2022R5), Princess Nourah bint Abdulrahman University, Riyadh, Saudi Arabia.

**Conflicts of Interest:** The authors declare no conflict of interest.

## References

1. Helmi, F.; Helmi, M.; Hemmati, A. Phosphomolybdic Acid/Chitosan as Acid Solid Catalyst Using for Biodiesel Production from Pomegranate Seed Oil via Microwave Heating System: RSM Optimization and Kinetic Study. *Renew. Energy* **2022**, *189*, 881–898. [[CrossRef](#)]
2. Lima, A.C.; Hachemane, K.; Ribeiro, A.E.; Queiroz, A.; Gomes, M.C.S.; Brito, P. Evaluation and Kinetic Study of Alkaline Ionic Liquid for Biodiesel Production through Transesterification of Sunflower Oil. *Fuel* **2022**, *324*, 124586. [[CrossRef](#)]
3. Alismaeel, Z.T.; Al-Jadir, T.M.; Albayati, T.M.; Abbas, A.S.; Doyle, A.M. Modification of FAU Zeolite as an Active Heterogeneous Catalyst for Biodiesel Production and Theoretical Considerations for Kinetic Modeling. *Adv. Powder Technol.* **2022**, *33*, 103646. [[CrossRef](#)]
4. Lee, J.H.; Jeon, H.; Park, J.T.; Kim, J.H. Synthesis of Hierarchical Flower-Shaped Hollow MgO Microspheres via Ethylene-Glycol-Mediated Process as a Base Heterogeneous Catalyst for Transesterification for Biodiesel Production. *Biomass Bioenergy* **2020**, *142*, 105788. [[CrossRef](#)]
5. Yatish, K.V.; Omkaresh, B.R.; Kattimani, V.R.; Lalithamba, H.S.; Sakar, M.; Balakrishna, R.G. Solar Energy-Assisted Reactor for the Sustainable Biodiesel Production from Butea Monosperma Oil: Optimization, Kinetic, Thermodynamic and Assessment Studies. *Energy* **2023**, *263*, 125768. [[CrossRef](#)]
6. Rabie, A.M.; Shaban, M.; Abukhadra, M.R.; Hosny, R.; Ahmed, S.A.; Negm, N.A. Diatomite Supported by CaO/MgO Nanocomposite as Heterogeneous Catalyst for Biodiesel Production from Waste Cooking Oil. *J. Mol. Liq.* **2019**, *279*, 224–231. [[CrossRef](#)]
7. Wu, L.; Wei, T.Y.; Tong, Z.F.; Zou, Y.; Lin, Z.J.; Sun, J.H. Bentonite-Enhanced Biodiesel Production by NaOH-Catalyzed Transesterification of Soybean Oil with Methanol. *Fuel Process. Technol.* **2016**, *144*, 334–340. [[CrossRef](#)]
8. Sultana, N.; Das, A.; Guria, C.; Hajra, B.; Chitres, G.; Saxena, V.K.; Pathak, A.K. Kinetics of Bentonite Nanoclay-Catalyzed Sal Oil (*Shorea Robusta*) Transesterification with Methanol. *Chem. Eng. Res. Des.* **2017**, *119*, 263–285. [[CrossRef](#)]
9. Salim, S.M.; Izriq, R.; Almaky, M.M.; Al-Abbassi, A.A. Synthesis and Characterization of ZnO Nanoparticles for the Production of Biodiesel by Transesterification: Kinetic and Thermodynamic Studies. *Fuel* **2022**, *321*, 124135. [[CrossRef](#)]
10. Lawan, I.; Garba, Z.N.; Zhou, W.; Zhang, M.; Yuan, Z. Synergies between the Microwave Reactor and CaO/Zeolite Catalyst in Waste Lard Biodiesel Production. *Renew. Energy* **2020**, *145*, 2550–2560. [[CrossRef](#)]
11. Zhong, L.; Feng, Y.; Wang, G.; Wang, Z.; Bilal, M.; Lv, H.; Jia, S.; Cui, J. Production and Use of Immobilized Lipases in/on Nanomaterials: A Review from the Waste to Biodiesel Production. *Int. J. Biol. Macromol.* **2020**, *152*, 207–222. [[CrossRef](#)] [[PubMed](#)]
12. Yang, X.-X.; Wang, Y.-T.; Yang, Y.-T.; Feng, E.-Z.; Luo, J.; Zhang, F.; Yang, W.-J.; Bao, G.-R. Catalytic Transesterification to Biodiesel at Room Temperature over Several Solid Bases. *Energy Convers. Manag.* **2018**, *164*, 112–121. [[CrossRef](#)]
13. Saravanan, A.; Karishma, S.; Senthil Kumar, P.; Jayasree, R. Process Optimization and Kinetic Studies for the Production of Biodiesel from Artocarpus Heterophyllus Oil Using Modified Mixed Quail Waste Catalyst. *Fuel* **2022**, *330*, 125644. [[CrossRef](#)]
14. Tang, Z.E.; Lim, S.; Pang, Y.L.; Shuit, S.H.; Ong, H.C. Utilisation of Biomass Wastes Based Activated Carbon Supported Heterogeneous Acid Catalyst for Biodiesel Production. *Renew. Energy* **2020**, *158*, 91–102. [[CrossRef](#)]
15. Mahlia, T.M.I.; Syazmi, Z.A.H.S.; Mofijur, M.; Abas, A.E.P.; Bilad, M.R.; Ong, H.C.; Silitonga, A.S. Patent Landscape Review on Biodiesel Production: Technology Updates. *Renew. Sustain. Energy Rev.* **2020**, *118*, 109526. [[CrossRef](#)]
16. Wang, Y.T.; Yang, X.X.; Xu, J.; Wang, H.L.; Wang, Z.B.; Zhang, L.; Wang, S.L.; Liang, J.L. Biodiesel Production from Esterification of Oleic Acid by a Sulfonated Magnetic Solid Acid Catalyst. *Renew. Energy* **2019**, *139*, 688–695. [[CrossRef](#)]
17. Fereidooni, L.; Abbaspourrad, A.; Enayati, M. Electrolytic Transesterification of Waste Frying Oil Using Na<sup>+</sup>/Zeolite–Chitosan Biocomposite for Biodiesel Production. *Waste Manag.* **2021**, *127*, 48–62. [[CrossRef](#)]
18. Sayed, M.R.; Abukhadra, M.R.; Abdelkader Ahmed, S.; Shaban, M.; Javed, U.; Betiha, M.A.; Shim, J.J.; Rabie, A.M. Synthesis of Advanced MgAl-LDH Based Geopolymer as a Potential Catalyst in the Conversion of Waste Sunflower Oil into Biodiesel: Response Surface Studies. *Fuel* **2020**, *282*, 118865. [[CrossRef](#)]
19. Jumah, M.N.B.; Ibrahim, S.M.; AL-Huqail, A.A.; Bin-Murdhi, N.S.; Allam, A.A.; Abu-Taweel, G.M.; Altoom, N.; Al-Anazi, K.M.; Abukhadra, M.R. Enhancing the Catalytic Performance of NiO during the Transesterification of Waste Cooking Oil Using a Diatomite Carrier and an Integrated NiO Metal: Response Surface Studies. *ACS Omega* **2021**, *6*, 12318–12330. [[CrossRef](#)]
20. Sahu, O. Characterisation and Utilization of Heterogeneous Catalyst from Waste Rice-Straw for Biodiesel Conversion. *Fuel* **2021**, *287*, 119543. [[CrossRef](#)]
21. Singh, V.; Bux, F.; Sharma, Y.C. A Low Cost One Pot Synthesis of Biodiesel from Waste Frying Oil (WFO) Using a Novel Material,  $\beta$ -Potassium Dizirconate ( $\beta$ -K<sub>2</sub>Zr<sub>2</sub>O<sub>5</sub>). *Appl. Energy* **2016**, *172*, 23–33. [[CrossRef](#)]
22. Abukhadra, M.R.; Soliman, S.R.; Bin Jumah, M.N.; Othman, S.I.; AlHammadi, A.A.; Alruhaimi, R.S.; Albohairy, F.M.; Allam, A.A. Insight into the Sulfonation Conditions on the Activity of Sub-Bituminous Coal as Acidic Catalyst during the Transesterification of Spent Corn Oil; Effect of Sonication Waves. *Sustain. Chem. Pharm.* **2022**, *27*, 100691. [[CrossRef](#)]

23. Dăng, T.H.; Chen, B.H.; Lee, D.J. Optimization of Biodiesel Production from Transesterification of Triolein Using Zeolite LTA Catalysts Synthesized from Kaolin Clay. *J. Taiwan Inst. Chem. Eng.* **2017**, *79*, 14–22. [[CrossRef](#)]
24. Otieno, S.O.; Kowenje, C.O.; Okoyo, A.; Onyango, D.M.; Amisi, K.O.; Nzioka, K.M. Optimizing Production of Biodiesel Catalysed by Chemically Tuned Natural Zeolites. *Mater. Today Proc.* **2018**, *5*, 10561–10569. [[CrossRef](#)]
25. Du, L.; Ding, S.; Li, Z.; Lv, E.; Lu, J.; Ding, J. Transesterification of Castor Oil to Biodiesel Using NaY Zeolite-Supported La<sub>2</sub>O<sub>3</sub> Catalysts. *Energy Convers. Manag.* **2018**, *173*, 728–734. [[CrossRef](#)]
26. Fattahi, N.; Triantafyllidis, K.; Luque, R.; Ramazani, A. Zeolite-Based Catalysts: A Valuable Approach toward Ester Bond Formation. *Catalysts* **2019**, *9*, 758. [[CrossRef](#)]
27. Nasief, F.M.; Shaban, M.; Alamry, K.A.; Khadra, M.R.A.; Khan, A.A.P.; Asiri, A.M.; El-Salam, H.M.A. Hydrothermal Synthesis and Mechanically Activated Zeolite Material for Utilizing the Removal of Ca/Mg from Aqueous and Raw Groundwater. *J. Environ. Chem. Eng.* **2021**, *9*, 105834. [[CrossRef](#)]
28. Simanjuntak, W.; Pandiangan, K.D.; Sembiring, Z.; Simanjuntak, A.; Hadi, S. The Effect of Crystallization Time on Structure, Microstructure, and Catalytic Activity of Zeolite-A Synthesized from Rice Husk Silica and Food-Grade Aluminum Foil. *Biomass Bioenergy* **2021**, *148*, 106050. [[CrossRef](#)]
29. Altoom, N.; Adlii, A.; Othman, S.I.; Allam, A.A.; Alqhtani, H.A.; Al-Otaibi, F.S.; Abukhadra, M.R. Synthesis and Characterization of  $\beta$ -Cyclodextrin Functionalized Zeolite-A as Biocompatible Carrier for Levofloxacin Drug; Loading, Release, Cytotoxicity, and Anti-Inflammatory Studies. *J. Solid State Chem.* **2022**, *312*, 123280. [[CrossRef](#)]
30. Pandiangan, K.D.; Simanjuntak, W.; Pratiwi, E.; Rilyanti, M. Characteristics and Catalytic Activity of Zeolite-a Synthesized from Rice Husk Silica and Aluminium Metal by Sol-Gel Method. *J. Phys. Conf. Ser.* **2019**, *1338*, 012015. [[CrossRef](#)]
31. Abukhadra, M.R.; Sayed, M.A. K<sup>+</sup> Trapped Kaolinite (Kaol/K<sup>+</sup>) as Low Cost and Eco-Friendly Basic Heterogeneous Catalyst in the Transesterification of Commercial Waste Cooking Oil into Biodiesel. *Energy Convers. Manag.* **2018**, *177*, 468–476. [[CrossRef](#)]
32. Dardir, F.M.; Mohamed, A.S.; Abukhadra, M.R.; Ahmed, E.A.; Soliman, M.F. Cosmetic and Pharmaceutical Qualifications of Egyptian Bentonite and Its Suitability as Drug Carrier for Praziquantel Drug. *Eur. J. Pharm. Sci.* **2018**, *115*, 320–329. [[CrossRef](#)]
33. Roy, T.; Sahani, S.; Chandra Sharma, Y. Study on Kinetics-Thermodynamics and Environmental Parameter of Biodiesel Production from Waste Cooking Oil and Castor Oil Using Potassium Modified Ceria Oxide Catalyst. *J. Clean. Prod.* **2020**, *247*, 119166. [[CrossRef](#)]
34. Ayele, L.; Pérez-Pariente, J.; Chebude, Y.; Díaz, I. Conventional versus Alkali Fusion Synthesis of Zeolite A from Low Grade Kaolin. *Appl. Clay Sci.* **2016**, *132–133*, 485–490. [[CrossRef](#)]
35. Ashraf, M.T.; AlHammadi, A.A.; El-Sherbeeney, A.M.; Alhammadi, S.; Al Zoubi, W.; Ko, Y.G.; Abukhadra, M.R. Synthesis of Cellulose Fibers/Zeolite-A Nanocomposite as an Environmental Adsorbent for Organic and Inorganic Selenium Ions; Characterization and Advanced Equilibrium Studies. *J. Mol. Liq.* **2022**, *360*, 119573. [[CrossRef](#)]
36. AbuKhadra, M.R.; Basyouny, M.G.; El-Sherbeeney, A.M.; El-Meligy, M.A.; Abd Elgawad, A.E.E. Transesterification of Commercial Waste Cooking Oil into Biodiesel over Innovative Alkali Trapped Zeolite Nanocomposite as Green and Environmental Catalysts. *Sustain. Chem. Pharm.* **2020**, *17*, 100289. [[CrossRef](#)]
37. Mostafa, M.; El-Meligy, M.A.; Sharaf, M.; Soliman, A.T.; AbuKhadra, M.R. Insight into Chitosan/Zeolite-A Nanocomposite as an Advanced Carrier for Levofloxacin and Its Anti-Inflammatory Properties; Loading, Release, and Anti-Inflammatory Studies. *Int. J. Biol. Macromol.* **2021**, *179*, 206–216. [[CrossRef](#)] [[PubMed](#)]
38. Basyouny, M.G.; Abukhadra, M.R.; Alkhaledi, K.; El-Sherbeeney, A.M.; El-Meligy, M.A.; Soliman, A.T.A.; Luqman, M. Insight into the Catalytic Transformation of the Waste Products of Some Edible Oils (Corn Oil and Palm Oil) into Biodiesel Using MgO/Clinoptilolite Green Nanocomposite. *Mol. Catal.* **2021**, *500*, 111340. [[CrossRef](#)]
39. Toledo Arana, J.; Torres, J.J.; Acevedo, D.F.; Illanes, C.O.; Ochoa, N.A.; Pagliero, C.L. One-Step Synthesis of CaO-ZnO Efficient Catalyst for Biodiesel Production. *Int. J. Chem. Eng.* **2019**, *2019*, 1806017. [[CrossRef](#)]
40. Gardy, J.; Rehan, M.; Hassanpour, A.; Lai, X.; Nizami, A.S. Advances in Nano-Catalysts Based Biodiesel Production from Non-Food Feedstocks. *J. Environ. Manage.* **2019**, *249*, 109316. [[CrossRef](#)]
41. Seela, C.R.; Alagumalai, A.; Pugazhendhi, A. Evaluating the Feasibility of Diethyl Ether and Isobutanol Added Jatropha Curcas Biodiesel as Environmentally Friendly Fuel Blends. *Sustain. Chem. Pharm.* **2020**, *18*, 100340. [[CrossRef](#)]
42. Bhatia, S.K.; Gurav, R.; Choi, T.R.; Kim, H.J.; Yang, S.Y.; Song, H.S.; Park, J.Y.; Park, Y.L.; Han, Y.H.; Choi, Y.K.; et al. Conversion of Waste Cooking Oil into Biodiesel Using Heterogenous Catalyst Derived from Cork Biochar. *Bioresour. Technol.* **2020**, *302*, 122872. [[CrossRef](#)] [[PubMed](#)]
43. Hassan, W.A.; Ahmed, E.A.; Moneim, M.A.; Shaban, M.S.; El-Sherbeeney, A.M.; Siddiqui, N.; Shim, J.J.; Abukhadra, M.R. Sulfonation of Natural Carbonaceous Bentonite as a Low-Cost Acidic Catalyst for Effective Transesterification of Used Sunflower Oil into Diesel; Statistical Modeling and Kinetic Properties. *ACS Omega* **2021**, *6*, 31260–31271. [[CrossRef](#)] [[PubMed](#)]
44. Abukhadra, M.R.; Othman, S.I.; Allam, A.A.; Elfayoumi, H. Insight into the Catalytic Properties Zeolitized Kaolinite/Diatomite Geopolymer as an Environmental Catalyst for the Sustainable Conversion of Spent Cooking Oil into Biodiesel; Optimization and Kinetics. *Sustain. Chem. Pharm.* **2021**, *22*, 100473. [[CrossRef](#)]
45. Mumtaz, M.W.; Adnan, A.; Anwar, F.; Mukhtar, H.; Raza, M.A.; Ahmad, F.; Rashid, U. Response Surface Methodology: An Emphatic Tool for Optimized Biodiesel Production Using Rice Bran and Sunflower Oils. *Energies* **2012**, *5*, 3307–3328. [[CrossRef](#)]
46. Kamel, D.A.; Farag, H.A.; Amin, N.K.; Zatout, A.A.; Ali, R.M. Smart Utilization of Jatropha (*Jatropha Curcas* Linnaeus) Seeds for Biodiesel Production: Optimization and Mechanism. *Ind. Crops Prod.* **2018**, *111*, 407–413. [[CrossRef](#)]

47. Kouzu, M.; Kasuno, T.; Tajika, M.; Sugimoto, Y.; Yamanaka, S.; Hidaka, J. Calcium Oxide as a Solid Base Catalyst for Transesterification of Soybean Oil and Its Application to Biodiesel Production. *Fuel* **2008**, *87*, 2798–2806. [[CrossRef](#)]
48. Li, Z.; Ding, S.; Chen, C.; Qu, S.; Du, L.; Lu, J.; Ding, J. Recyclable Li/NaY Zeolite as a Heterogeneous Alkaline Catalyst for Biodiesel Production: Process Optimization and Kinetics Study. *Energy Convers. Manag.* **2019**, *192*, 335–345. [[CrossRef](#)]
49. Yusuff, A.S.; Bhonsle, A.K.; Bangwal, D.P.; Atray, N. Development of a Barium-Modified Zeolite Catalyst for Biodiesel Production from Waste Frying Oil: Process Optimization by Design of Experiment. *Renew. Energy* **2021**, *177*, 1253–1264. [[CrossRef](#)]
50. Yusuff, A.S.; Gbadamosi, A.O.; Atray, N. Development of a Zeolite Supported CaO Derived from Chicken Eggshell as Active Base Catalyst for Used Cooking Oil Biodiesel Production. *Renew. Energy* **2022**, *197*, 1151–1162. [[CrossRef](#)]
51. Lani, N.S.; Ngadi, N.; Inuwa, I.M.; Opotu, L.A.; Zakaria, Z.Y.; Widayat, W. Influence of Desilication Route of ZSM-5 Zeolite in Mesoporous Zeolite Supported Calcium Oxide Catalyst for Biodiesel Production. *Microporous Mesoporous Mater.* **2022**, *343*, 112153. [[CrossRef](#)]
52. Chen, G.; Shan, R.; Li, S.; Shi, J. A Biomimetic Silicification Approach to Synthesize CaO-SiO<sub>2</sub> Catalyst for the Transesterification of Palm Oil into Biodiesel. *Fuel* **2015**, *153*, 48–55. [[CrossRef](#)]
53. Aghel, B.; Mohadesi, M.; Ansari, A.; Maleki, M. Pilot-Scale Production of Biodiesel from Waste Cooking Oil Using Kettle Limescale as a Heterogeneous Catalyst. *Renew. Energy* **2019**, *142*, 207–214. [[CrossRef](#)]
54. Babajide, O.; Musyoka, N.; Petrik, L.; Ameer, F. Novel Zeolite Na-X Synthesized from Fly Ash as a Heterogeneous Catalyst in Biodiesel Production. *Catal. Today* **2012**, *190*, 54–60. [[CrossRef](#)]
55. Maneerung, T.; Kawi, S.; Wang, C.H. Biomass Gasification Bottom Ash as a Source of CaO Catalyst for Biodiesel Production via Transesterification of Palm Oil. *Energy Convers. Manag.* **2015**, *92*, 234–243. [[CrossRef](#)]
56. Amani, H.; Asif, M.; Hameed, B.H. Transesterification of Waste Cooking Palm Oil and Palm Oil to Fatty Acid Methyl Ester Using Cesium-Modified Silica Catalyst. *J. Taiwan Inst. Chem. Eng.* **2016**, *58*, 226–234. [[CrossRef](#)]
57. Thushari, I.; Babel, S.; Samart, C. Biodiesel Production in an Autoclave Reactor Using Waste Palm Oil and Coconut Coir Husk Derived Catalyst. *Renew. Energy* **2019**, *134*, 125–134. [[CrossRef](#)]

**Disclaimer/Publisher’s Note:** The statements, opinions and data contained in all publications are solely those of the individual author(s) and contributor(s) and not of MDPI and/or the editor(s). MDPI and/or the editor(s) disclaim responsibility for any injury to people or property resulting from any ideas, methods, instructions or products referred to in the content.